Theoret.Appl.Mech. TEOPM7, Vol.41, No.1, pp.1–35, Belgrade 2014 *

FINITE ELEMENT AND NETWORK ELECTRICAL SIMULATION OF ROTATING MAGNETOFLUID FLOW IN NONLINEAR POROUS MEDIA WITH INCLINED MAGNETIC FIELD AND HALL CURRENTS

O. Anwar Bég S. Rawat J.Zueco
L.Osmond R.S.R.Gorla

*doi:10.2298/TAM1401037P Math. Subj. Class.: 76E06; 76S05; 76W05; 76M20.

According to: *Tib Journal Abbreviations (C) Mathematical Reviews*, the abbreviation TEOPM7 stands for TEORIJSKA I PRIMENJENA MEHANIKA.

Theoret. Appl. Mech., Vol.41, No.1, pp.1–35, Belgrade 2014

Finite element and network electrical simulation of rotating magnetofluid flow in nonlinear porous media with inclined magnetic field and Hall currents

O. Anwar Bég* S. Rawat† J.Zueco‡
L.Osmond § R.S.R.Gorla ¶

Abstract

A mathematical model is presented for viscous hydromagnetic flow through a hybrid non-Darcy porous media rotating generator. The system is simulated as steady, incompressible flow through a nonlinear porous regime intercalated between parallel plates of the generator in a rotating frame of reference in the presence of a strong, inclined magnetic field A pressure gradient term is included which is a function of the longitudinal coordinate. The general equations for rotating viscous magnetohydrodynamic flow are presented and neglecting convective acceleration effects, the two-dimensional viscous flow equations are derived incorporating current density components, porous media drag effects, Lorentz drag force components and Hall current effects. Using an appropriate group of dimensionless variables, the momentum equations for primary and secondary flow are rendered non-dimensional and shown to be controlled by six physical parameters- Hartmann number (Ha), Hall current parameter (Nh), Darcy number (Da), Forchheimer number (Fs), Ekman number (Ek) and dimensionless pressure gradient parameter (Np), in addition to one geometric parameter- the orientation of the applied magnetic field (θ). Several special cases are extracted from the general model, including the non-porous case studied earlier by Ghosh and Pop (2006). A numerical solution is presented to the

*Gort Engovation(Propulsion and Biomechanics), Southmere Avenue., Bradford, BD7 3NU, England, UK, email: gortoab@gmail.com

†Department of Mathematics, Galgotias University, Greater Noida, UP, India and Department of Mathematics, Jubail University College (Male Branch)Jubail Industrial City 31961,Kingdom of Saudi Arabia

‡Departamento de Ingenieria Termica y Fluidos, Universidad Politecnica de Cartagena, Murcia, Spain

§Energy Institute, School of Engineering, Leeds University, Leeds, LS29JT, England, UK

¶Mechanical Engineering, Cleveland State University, Cleveland, Ohio, USA

nonlinear coupled ordinary differential equations using both the **Network Simulation Method** and **Finite Element Method**, achieving excellent agreement. Additionally very good agreement is also obtained with the earlier analytical solutions of Ghosh and Pop (2006). for selected Ha, Ek and Nh values. We examine in detail the effects of magnetic field, rotation, Hall current, bulk porous matrix drag, second order porous impedance, pressure gradient and magnetic field inclination on primary and secondary velocity distributions and also frictional shear stresses at the plates. Primary velocity is seen to decrease with an increase in Hall current parameter (Nh) with the converse observed for the secondary velocity.

Keywords: Magnetohydrodynamics (MHD); inclined field; porous regime; Forchheimer number; Ekman number; Hall currents; plasma; numerical; network simulation; finite element method; propulsion

1 Introduction

The Magnetohydrodynamic (MHD) generator has been developed for some time and has undergone major modifications to increase efficiency. It has been customized to the novel MPD thrusters developed by NASA. A lucid review of state-of-the-art developments has been conducted recently by Osmond [1]. Early studies of MHD generators focused on the *Faraday* generator. Unfortunately in such generators, there is a tendency for differential voltages and currents in the fluid to short through the electrodes on the sides of the duct, often due to the presence of *Hall currents*. As such the Faraday MHD duct generator [2, 3] has a greatly reduced efficiency. Although very powerful super-conducting magnets may be employed to improve the Faraday MHD generator efficiency, a more effective and economically viable mechanism is to utilize the *Hall effect* to generate a current which flows with the fluid, which is often achieved by implementing groups of short, vertical electrodes on the sides of the generator duct [4]. These shorts of the Faraday current generate a strong magnetic field within the fluid and this secondary, induced field produces current flow in a "rainbow shape" between the first and last electrodes. As a result energy losses are significantly less than with the conventional MHD Faraday generator, and voltages are higher because there is less shorting of the final induced current. On the other hand this mechanism also creates some new inefficiency problems since the velocity of the working fluid requires the middle electrodes to be offset to "catch" the Faraday currents. When the load varies, the fluid flow velocity is affected resulting in misalignment of the Faraday current with its intended electrodes, and reducing the generator's efficiency. A key problem is to stabilize the hydro-magnetic flow in such systems. Porous media may successfully achieve

this; the present study aims to address this problem mathematically and numerically. Under *low strength* magnetic fields, the electrically-conducting "working" fluid can be simulated usually by augmenting the Navier-Stokes equations with a Lorentzian body force term [5]. Numerous researchers have investigated a wide variety of magnetohydrodynamic energy flow problems in purely fluid media. Inui et al [6] studied the non-equilibrium disk MHD generator flow regime Al-Nimr [7] studied hydro-magnetic flow and heat transfer in annular regimes with wall suction. Chatuverdi [8] investigated the influence of exponential variation of suction velocity and free stream velocity with time on hydromagnetic flat plate flow. Inoue et al [9] investigated the CDIF (Component Development Integration Facility) MHD generator theoretically. Chen et al [10] considered the heat transfer effect on the performance of MHD power plant under constant Mach number conditions. Ishikawa et al [11] studied magnetic induction effects in two-phase hydromagnetic flow in a large scale pulsed MHD generator. Very recently Aïboud-Saouli et al [12] reported on the entropy generation in hydro-magnetic fully-developed channel flow with heat generation and viscous dissipation effects.With high magnetic field strengths, supplementary effects arise in MHD generator systems including Hall currents, ionslip effects, Alfven waves, Landau damping etc. Considerable attention has been devoted to analyzing theoretically and numerically a wide range of MHD flows with *Hall current* effects in various simple geometrical scenarios. In partially ionized fluids (e.g. water solution seeded with Potassium) which occur in MHD energy systems, Hall currents can have a significant effect on the flow development. The presence of longitudinal Hall currents in a flow creates a transverse body force which can lead to transverse pressure gradients, velocity gradients etc [5]. Sato [13] presented one of the earliest analyzes for Hall current effects in parallel plate viscous MHD flow. Other studies assessing hydromagnetic flows with Hall current effects include those by Yamanishi [14], Katagiri [15], Pop and Soundalgekar [16] and Gupta [17], the latter two analyses also incorporating suction/injection effects. Masapati et al [18] studied the influence of Hall and ionslip currents on hydromagnetic entry channel flow. Bhat and Mittal [19] later investigated the heat transfer regime with uniform wall heat flux in the developing flow region in the presence of Hall and ionslip currents. Soundalgekar et. al. [20] obtained numerical solutions for hydro-magnetic Couette flow and convection with Hall and Ionslip currents. Singh [21] presented one of the first papers on *transient* MHD flow with Hall currents for the Stokes problem past an infinite porous vertical surface. Kinyanjui et al [22] studied hydro-magnetic natural convection heat and mass transfer with Hall current and radiation effects considering both the cooled and heated plate scenarios. These investigations did not consider *rotational* effects. In MHD generator system flows, rotation can exert a significant

influence on the fluid dynamics of the system. Nanda and Mohanty [23] probably were the first to perform a rigorous analysis of steady hydro-magnetic rotating channel flow. Their exact solutions indicated that for high Hartmann and low Ekman numbers, *thin boundary layer*s are generated on the channel wall interiors.Soundalgekar and Bhat [24] presented exact solutions for hydro-magnetic viscous flow in a rotating channel with magnetic induction effects, showing that the velocity field is strongly affected by the sum of the electrical conductance ratios of the two plates. Arikoglu et al [25] investigated numerically the influence of slip on entropy generation in hydro-magnetic flow from a rotating disk, showing that with a minimzed entropy generation, equipartitioning is encountered between the fluid friction irreversibility and Joule dissipation. Bég *et al* [26] used an implicit difference method to study the combined effects of buoyancy and impulsive motion on hydro-magnetic convection boundary layer flow from a spinning sphere. Very recently Ghosh et al [27] analyzed thermal radiation effects on rotating hydro-magnetic gas flow from a vertical plate. Rotating hydro-magnetic flows with Hall current effects have also received some attention owing to application in the MHD rotating generator system. Takhar et al [28] studied analytically the Strouhal and Hartmann number effects on transient rotating hydro-magnetic channel flow of a dusty fluid. Myoshi and Kusano [29] considered the rapidly rotating magnetohydrodynamic flow from a sphere with an external plasma flow including Hall currents. Ram et al [30] studied the effects of Hall and ionslip currents on MHD rotating convection using a finite difference method. Takhar and Jha [31] considered the impulsively-started hydro-magnetic rotating flow from a vertical plane with Hall and ionslip effects.Kinyanjui et al [32] employed a finite difference method to study hydro-magnetic Stokes flow problem for a vertical infinite plate in a dissipative rotating fluid with Hall current, for the case of cooling of the plate by free convection currents. Takhar et al [33] later reported on free stream effects on magneto-hydrodynamic rotating flow over a translating surface. Naroua et al [34] more recently studied the heat generation/absorption effects on transient MHD convection of a gas in a rotating system with Hall/ionslip effects using finite element analysis. Generally in studies concerning rotating hydro-magnetic flow the applied magnetic field has been assumed to be *normal* to the primary flow. However the effects of *inclined magnetic field* are especially significant in establishing the optimum performance of MHD plasma devices and also in the context of operation of MHD generators. Several articles have addressed *rotating hydro-magnetic flows* with an inclined magnetic field including the study by Ghosh [35] which included the influence of an oscillator and Hall effects and more recently the analysis by Ghosh and Pop [36] which presented closed-form solutions for steady MHD rotating plasma flow under inclined magnetic fields in the context of solar hydro-magnetics. The

above investigations have been restricted to purely fluid regimes. Porous media may be exploited to achieve enhanced flow control in MHD energy systems. The majority of porous fluid dynamics studies with or without magnetic fields have employed the *Darcy law*, which is an empirical linear relation between the pressure drop across the porous medium and the viscous and gravitational forces. Bear [37] provides an excellent discussion of Darcian flows. In high-velocity scenarios, the influence of inertial effects may become significant. To model such a phenomenon the *Darcy-Forchheimer non-linear drag force model* is widely used and can simulate therefore porous media flows where the Reynolds number based on the mean pore size is greater than unity. The pressure gradient across the porous medium is a quadratic relation with the volume averaged velocity.Takhar *et al* [38] studied Forchheimer drag effects on steady, incompressible biomagnetic flow in a porous medium. Magnetohydrodynamic flow in porous media has also received some attention. Takhar and Ram [39] discussed hydro-magnetic free convection in porous media with Hall current effects using the Darcian model. Prasad *et al* [40] studied numerically the MHD flow in a Darcian rotating porous regime under inclined magnetic field with Hall effects. In the present study we extend the study by Ghosh and Pop [36] to incorporate *porous medium* effects using the Darcy-Forchheimer model. A full numerical solution using both Network Simulation Methodology (NSM) and the Finite Element Method (FEM) is developed and the effects of *Hartmann number (Ha), Hall current parameter (Nh), Darcy number (Da), Forchheimer number (Fs), Ekman number (Ek) and dimensionless pressure gradient parameter (Np)*, in addition to the *orientation of the applied magnetic field* (θ) on primary and secondary flow fields is considered. Such a study has to the authors' knowledge thusfar not received attention in the scientific literature and find important applications in the use of porous media to control MHD rotating thruster/generator flow dynamics under strong magnetic field. In a subsequent study we employ the model to compute thrust specifications.

2 Mathematical model

The fundamental equations of magnetohydrodynamics in a rotating frame of reference, following Sutton and Sherman [5] can be shown to take the following form:

Hydromagnetic momentum conservation (Navier-Stokes) in rotating frame of reference:

$$(q \cdot \nabla)q \; + \; 2\Omega \hat{K} \times q = -\frac{1}{\rho}\nabla p + \nu \nabla^2 q + \frac{1}{\rho} J \times B \tag{1}$$

Mass Conservation

$$\vec{\nabla} \cdot q = 0 \tag{2}$$

Oh's Law for moving conductor with Hall currents:

$$J + \frac{\omega_e \tau_e}{B_o}(J \times B) = \sigma[E + q \times B] \tag{3}$$

Maxwell Electromagnetic Equations:

$$\vec{\nabla} \cdot B = \mu_e J \tag{4}$$

$$\vec{\nabla} \cdot E = -\frac{\partial B}{\partial t} \tag{5}$$

$$\vec{\nabla} \cdot J \neq 0 \tag{6}$$

$$\vec{\nabla} \cdot D = \rho_e \tag{7}$$

$$\vec{\nabla} \cdot B = 0 \tag{8}$$

where q is velocity vector, B is magnetic field vector, E denotes electrical field vector, $\boldsymbol{J}$ is current density vector and D is the displacement vector, $\vec{K}$ is unit vector along the z-axis, p is pressure,ρ is density of the working fluid, ν is kinematic viscosity, ω_e is the cyclotron frequency, τ_e is electron collision time, σ is the electrical conductivity of the working fluid and μ_e is the magnetic permeability. We consider the steady magnetohydrodynamic viscous incompressible, partially-ionized fluid in nonlinear isotropic, homogenous, porous medium intercalated between two parallel infinitely long plates, rotating with constant angular velocity,Ω, in an $x - y$ plane, in the presence of a strong magnetic field inclined to the positive direction of the *z-axis* (axis of rotation, normal to the x-y plane). The plates are therefore located at $z = L$ *and* z= -L. The fluid-saturated regime and the plate are assumed to be in a state of *rigid rotation.* They both possess a uniform angular velocity, , about the *z-axis*, which is perpendicular to the plates. A constant pressure gradient is applied to the flow. The magnetic Reynolds number is small for the partially-ionized plasma so that magnetic induction effects can be ignored. However, relative motion of the particles in the fluid can occur. As such, an electric current density, $\boldsymbol{J}$, is required to represent the relative motion of charged particles. Considering only the electromagnetic forces on these particles, we can utilize the generalized Ohm law. Ionslip effects are however ignored in the analysis. The physical regime is shown in figure 1.

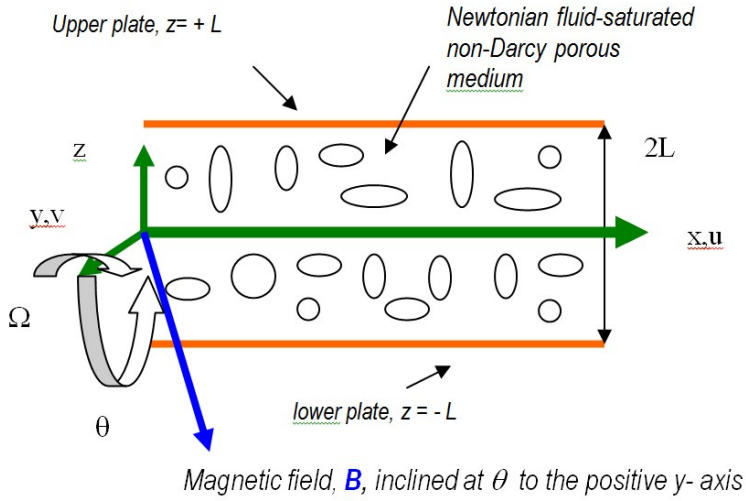

Figure 1: Physical Regime and Coordinate System

In the conservation equations (1) to (8), the velocity, magnetic field, electrical field and current density vectors are defined as:

$$q = (u', v', 0), \qquad \mathbf{B} = (B_x + BoSin\theta, B_y, B_oCos\theta),$$
$$E = (E_x, E_y, E_z), \qquad J = (J_x, J_y, J_z). \tag{9}$$

Due to the presence of Hall currents a *secondary flow* is induced and the flow domain is two-dimensional. Owing to the infinitely lengths of the plates in the $x-$ and y-directions, all physical variables with the exception of pressure are functions of the $z-$coordinate only. For steady state flow as considered in this paper, $\vec{\nabla} \cdot E = 0$. Following Ghosh and Pop [36], for continuous media equation (6) is valid for a discharge channel where the applied magnetic field is inclined to the rotation axis. For the present scenario, charge density, ρ_e, is minute and equation (7) reduces to $\vec{\nabla} \cdot D = 0$. In equations (1) to (9),Equation (8) is also known as the *solenoidal relation*. The porous medium is simulated using a *Darcy–Forcheimmer drag force model* which is a second order relationship defining the pressure gradient across the porous medium as:

$$\nabla p = -aU + bU^2 \tag{10}$$

where U denotes a volume-averaged velocity, ∇p is pressure gradient, a and b are constants defined by $a = \mu/K$ and b is a function of the geometry of porous medium (i.e. b is the Forcheimmer form-drag parameter for quadratic effects), μ

is the dynamic viscosity of the working fluid, K is permeability [hydraulic conductivity] of the porous medium. We have assumed that the porous medium is homogenous and isotropic so that only a single permeability is needed to simulate hydraulic conductivity. Under these physical conditions, the flow regime in the [x, y,z] coordinate system can be represented by the following simplified conservation equations, neglecting *convective acceleration* terms in the hydro-magnetic Navier-Stokes equations (1), viz:

x-direction Momentum Conservation

$$-2\Omega v' = -\frac{1}{\rho}\frac{\partial p}{\partial x} + \nu\frac{\partial^2 u'}{\partial z^2} + \frac{B_o}{\rho}J_y Cos\theta - \nu\frac{u'}{K} - b\frac{u'^2}{K} \tag{11}$$

y-direction Momentum Conservation

$$2\Omega u' = \nu\frac{\partial^2 v'}{\partial z^2} + \frac{B_o}{\rho}[J_y Sin\theta - J_x Cos\theta] - \nu\frac{v'}{K} - b\frac{v'^2}{K} \tag{12}$$

z-direction Momentum Conservation

$$0 = -\frac{1}{\rho}\frac{\partial p}{\partial z} - \frac{B_o}{\rho}J_y Sin\theta \tag{13}$$

To facilitate a numerical solution of the coupled, nonlinear partial differential equations (11) to (13) we introduce the following transformations:

$$\eta = \frac{z}{L} \tag{14}$$

$$u' = \frac{u\nu}{L} \tag{15}$$

$$v' = \frac{v\nu}{L} \tag{16}$$

$$Np = \frac{L^3}{\rho\nu^2}\left[-\frac{\partial p}{\partial x}\right] \tag{17}$$

$$Ek = \frac{\nu}{\Omega L^2} \tag{18}$$

$$Ha = B_o L[\frac{\sigma}{\rho\nu}]^{1/2} \tag{19}$$

$$Nh = \omega_e \tau_e \tag{20}$$

$$p = p' - \frac{1}{2}\rho\left|\Omega \times r\right|^2 \tag{21}$$

$$Da = \frac{K}{L^2} \tag{22}$$

$$Fs = \frac{b}{L} \tag{23}$$

where L denotes semi-channel depth, η is dimensionless z-coordinate, u is dimensionless x-direction velocity,v is dimensionless $y-$direction velocity, Np is the pressure gradient parameter, Ek is the Ekman number, Ha is the Hartmann number, Nh is the Hall current parameter, p is the dimensionless modified fluid pressure including centrifugal force, Da is the Darcy number, Fs is the Forchheimer number and r is the position vector from the axis of rotation. The momentum equations now reduce to the following simplified pair of coupled ordinary differential equations:

$$-2\frac{v}{Ek} = Np + \frac{d^2u}{d\eta^2} + \frac{Ha^2\cos\theta}{1+Nh^2}[Nhv - u\cos\theta] - \frac{u}{Da} - \frac{Fs}{Da}u^2 \tag{24}$$

$$2\frac{u}{Ek} = \frac{d^2v}{d\eta^2} - \frac{Ha^2}{1+Nh^2}[v + Nhu\cos\theta] - \frac{v}{Da} - \frac{Fs}{Da}v^2 \tag{25}$$

The corresponding transformed boundary conditions now become:

$$At\ \eta = +1\ (upper\ plate): \quad u = v = 0 \tag{26a}$$

$$At\ \eta = -1\ (lower\ plate): \quad u = v = 0 \tag{26b}$$

The ordinary differential equations (24) and (25) under boundary conditions (26a,b) constitute a robust two-point boundary value problem, which can be solved numerically. While we shall compute primary (u) and secondary (v) velocity profiles, we are also interested in evaluating the dimensionless frictional shear stresses at the plates, which are of interest from the viewpoint of industrial MHD energy system design (confining walls etc). These are given by the following relations for the primary and secondary flows:

$$\tau_{upper\,primary} = \left.\frac{du}{d\eta}\right|_{\eta=1} \tag{27a}$$

$$\tau_{lower\,primary} = \left.\frac{du}{d\eta}\right|_{\eta=-1} \tag{27b}$$

$$\tau_{upper\ \sec ondary} = \left.\frac{dv}{d\eta}\right|_{\eta=1} \tag{27c}$$

$$\tau_{lower\ \sec ondary} = \left.\frac{dv}{d\eta}\right|_{\eta=-1} \tag{27d}$$

In equations (24) and (25) the penultimate terms on the right hand side are the *x- direction Darcian drag force* and the *y-direction Darcian drag force*; the final terms on the right hand side of these equations designate the *Forcheimmer quadratic drag in the x-direction and y-direction respectively*.

3 Special cases

A number of special cases can be derived from the full transformed momentum equations (24), (25) which we shall now discuss

CASE I: Rotating MHD flow in non-Darcian regime under transverse magnetic field with Hall currents

With $\vartheta = 0$, $Cos\ 0 \to 1$, the inclined magnetic field is adjusted to be *normal* now to the plates i.e. parallel to the y-axis (rotation axis). The transport equations reduce therefore to:

$$-2\frac{v}{Ek} = Np + \frac{d^2u}{d\eta^2} + \frac{Ha^2}{1+Nh^2}[Nhv - u] - \frac{u}{Da} - \frac{Fs}{Da}u^2 \tag{28a}$$

$$2\frac{u}{Ek} = \frac{d^2v}{d\eta^2} - \frac{Ha^2}{1+Nh^2}[v + Nhu] - \frac{v}{Da} - \frac{Fs}{Da}v^2 \tag{28b}$$

Such a case constitutes much simpler MHD flow and is studied numerically in the present analysis.

CASE II: Rotating MHD flow in Darcian regime under inclined magnetic field with Hall current

With $Fs \to 0$, inertial effects disappear and only a linear bulk matrix resistance acts on the fluid in the porous medium. Both momentum equations (24) and (25) then reduce to:

$$-2\frac{v}{Ek} = Np + \frac{d^2u}{d\eta^2} + \frac{Ha^2\cos\theta}{1+Nh^2}[Nhv - u\cos\theta] - \frac{u}{Da} \tag{29a}$$

$$2\frac{u}{Ek} = \frac{d^2v}{d\eta^2} - \frac{Ha^2}{1+Nh^2}[v + Nhu\cos\theta] - \frac{v}{Da} \tag{29b}$$

CASE III: Rotating MHD flow in Darcian regime under Inclined magnetic field without Hall current

As $Nh \to 0$, Hall current effects vanish. The magnetic field parameter, Ha, in this case will have relatively small values. Case II can be further simplified now to yield:

$$-2\frac{v}{Ek} = Np + \frac{d^2u}{d\eta^2} + Ha^2\cos\theta[-u\cos\theta] - \frac{u}{Da} \tag{30a}$$

$$2\frac{u}{Ek} = \frac{d^2v}{d\eta^2} - Ha^2[v] - \frac{v}{Da} \tag{30b}$$

Clearly the flow fields are still coupled via the *rotational* terms on the left hand side of equations (30a) and (30b).

CASE IV: Rotating electrically non-conducting flow in non-Darcian regime

As $Ha \to 0$, magnetic drag force and Hall current effects vanish. The regime is then hydrodynamic rotating flow in a parallel plate system containing a non-Darcian porous medium. Equations (24) and (25) now take the form:

$$-2\frac{v}{Ek} = Np + \frac{d^2u}{d\eta^2} - \frac{u}{Da} - \frac{Fs}{Da}u^2 \tag{31a}$$

$$2\frac{u}{Ek} = \frac{d^2v}{d\eta^2} - \frac{v}{Da} - \frac{Fs}{Da}v^2 \tag{31b}$$

CASE V: Rotating MHD flow in purely fluid regime with Hall currents

As $Da \to \infty$, the permeability of the medium becomes infinite. In this limit, the material fibers vanish and the regime is now *non-porous*. Both Darcian and Forchheimer impedances vanish and equations (24) and (25) reduce to the form given by:

$$-2\frac{v}{Ek} = Np + \frac{d^2u}{d\eta^2} + \frac{Ha^2\cos\theta}{1+Nh^2}[Nhv - u\cos\theta] \tag{32a}$$

$$2\frac{u}{Ek} = \frac{d^2v}{d\eta^2} - \frac{Ha^2}{1+Nh^2}[v + Nhu\cos\theta] \tag{32b}$$

This linear case was studied analytically by Ghosh and Pop [36]. To compare the present numerical solutions we have reproduced the graphs of [36] for the variation of u and v with (for $Ha^2 = 10$, Ek = 0.25, Nh = 0 (i.e. Hall currents absent and strong rotation relative to weaker viscous forces)) in figures 2 and 3, in section 6.

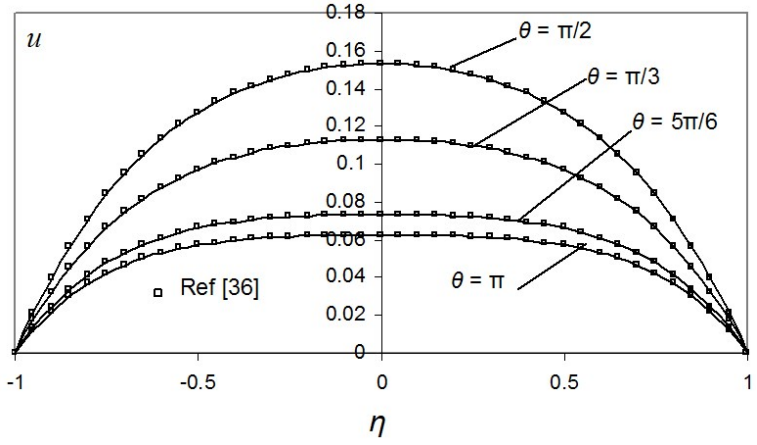

Figure 2: Velocity distribution (u) in the primary flow for $Ha^2 = 10$, Ek = 0.25, Np=1.0, Nh = 0 (NSM Method)

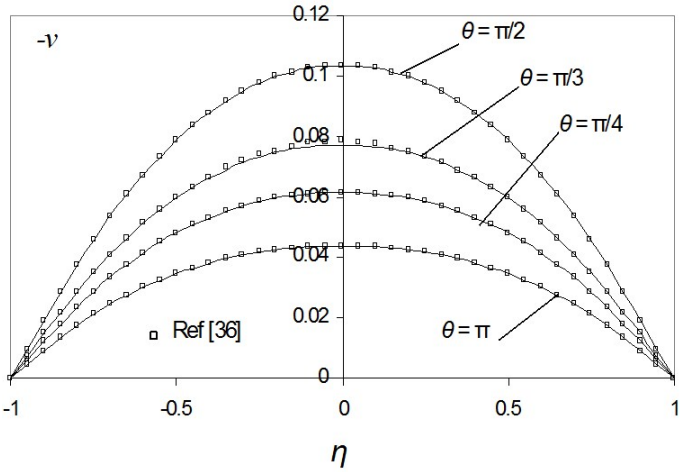

Figure 3: Velocity distribution (v) in the secondary flow for $Ha^2 = 10$, Ek = 0.25, Nh = 0 (NSM Method)

4 Network simulation method solutions

Numerical solutions to the governing transformed equations (24) and (25) subject to boundary conditions (26a,b,c) have been obtained using the Network Simulation Method (NSM) This method is a computationally-based solver with excellent accuracy, efficiency and reliability. NSM is based on the classical *thermoelectric analogy* between thermal and electrical variables. Nevertheless, its capacity to implement in the model any kind of non-linearity (due to boundary conditions, phase-change processes, temperature dependencies of the thermal properties, etc) distinguishes NSM from the analogies generally exposed in text books. NSM has been used in several recent studies by the authors and validated against other numerical methods including the Blottner implicit difference method. Bég et al [41] studied transient hydro-magnetic convection flow in a dissipative regime with Hall currents present, using NSM. Other studies employing NMS include thermal convection boundary layer flow in stratified porous media [42] and unsteady rotating non-Darcian Couette flow [43] The starting point in NSM is the set of finite-differential equations, one for each control volume, obtained by spatial discretization of the transformed equations (24) and (25). Based on these equations, a network model is designed, whose equations are formally equivalent to the discretized ones. The electrical analogy relates the electrical current (J) with the velocity fluxes ($\frac{\partial u}{\partial \eta}$ and $\frac{\partial v}{\partial \eta}$), while the electrical potential (Φ) is equivalent to u and v. A number of networks are connected

in series to make up the whole medium and boundary conditions are added by means of special electrical devices (current or voltage control-sources). Once the complete network model is designed, for which few programming rules are needed since not many devices form the network, a computer code (Pspice [44]) is used to simulate it providing the numerical solution. Using Fourier Law, the spatial discretization of eqs. (24) and (25) gives:

$$2\Delta\eta/Ekv_i + \Delta\eta Np + (u_{i\Delta\eta} - u_i)/(\Delta\eta/2) - (u_i - u_{i+\Delta\eta})/(\Delta\eta/2) + \Delta\eta H_a^2 cos\theta[Nhv_i cos\theta u_i]/(1+Nh^2) - \Delta\eta/Dau_i - \Delta\eta Fs/Dau_i^2 = 0 \quad (33)$$

$$(v_{i\Delta\eta} - v_i)/(\Delta\eta/2) - (v_i - v_{i+\Delta\eta})/(\Delta\eta/2) - 2\Delta\eta/Eku_i - \Delta\eta H_a^2[v_i + Nhcos\theta u_i]/(1+Nh^2) - \Delta\eta/Dav_i - \Delta\eta Fs/Dav_i^2 = 0 \quad (34)$$

The electrical analogy is applied to eqs.(33) and (34) together with Kirchhoff's law for the currents. To implement the boundary conditions at η= +1 and η= -1, constant voltage sources are employed for both velocities. The principal advantage of the NSM approach is that it avoids the necessity in traditional numerical difference schemes of manipulation of difference equations and the constraints of specified yardsticks around the convergence of numerical solutions.

5 Finite element method solutions

Numerical solutions to the governing transformed equations (24) and (25) subject to boundary conditions (26a,b,c) have also been obtained using the Finite Element Method. This is the most versatile numerical method employed by engineers. Bhargava et al [45] studied pulsating hydro-magnetic blood flow in porous media using FEM. Bég et al [41] investigated the non-Newtonian thermal convection flow from a porous plate to a Darcy-Forchheimer regime using FEM. Other studies utilizing FEM include biomagnetic thermal convection in porous media [47] and two-phase magnetohydrodynamic convection in a porous medium channel [48]. In FEM, the whole domain is initially discretized. In the present regime, the flow domain was therefore divided into a set of 160 line elements of equal width, each element being *two-noded*

5.1 Variational Formulation

The variational form associated with equations (24)-(25) over a typical two noded linear element (η_e, η_{e+1}) is given by:

$$\int_{\eta_e}^{\eta_{e+1}} w_1 \left\{ \frac{d^2u}{d\eta^2} - \frac{Ha^2\cos^2\theta}{1+Nh^2}u - \frac{u}{Da} - \frac{Fs}{Da}u^2 + 2\frac{v}{Ek} + \frac{Ha^2Nh\cos\theta}{1+Nh^2}\,v + Np \right\} d\eta = 0 \quad (35)$$

$$\int_{\eta_e}^{\eta_{e+1}} w_2 \left\{ \frac{d^2v}{d\eta^2} - \frac{Ha^2}{1+Nh^2}v - \frac{v}{Da} - \frac{Fs}{Da}v^2 - \frac{Ha^2Nh\cos\theta}{1+Nh^2}\,u - 2\frac{u}{Ek} \right\} d\eta = 0 \quad (36)$$

where w_1 *and* w_2 are arbitrary test functions and may be viewed as the variation in u *and* v respectively.

5.2 Finite Element Formulation

The finite element model may be obtained from equations (35)-(36) by substituting finite element approximations of the form:

$$u = \sum_{j=1}^{2} u_j\psi_j, \qquad v = \sum_{j=1}^{2} v_j\psi_j \quad (37)$$

with w_1=w_2 = ψ_i ($_i$= 1,2) where ψ_i are the shape functions for a typical element (η_e, η_{e+1}) and are taken as

$$\psi_1^{(e)} = \frac{\eta_{e+1}-\eta}{\eta_{e+1}-\eta_e}, \psi_2^{(e)} = \frac{\eta-\eta_e}{\eta_{e+1}-\eta_e} \eta_e \le \eta \le \eta_{e+1} \quad (38)$$

The finite element model of the equations thus formed is given by

$$\begin{bmatrix} [K^{11}] & [K^{12}] \\ [K^{21}] & [K^{22}] \end{bmatrix} \begin{bmatrix} \{u\} \\ \{v\} \end{bmatrix} = \begin{bmatrix} \{b^1\} \\ \{b^2\} \end{bmatrix} \quad (39)$$

where $[K^{mn}]$ and $[b^m]$ $(m, n = 1, 2)$ are the matrices of order 2×2 and 2×1

respectively. All these matrices may be defined as follows:

$$
\begin{aligned}
K_{ij}^{11} =& -\int_{\eta_e}^{\eta_{e+1}} \frac{d\psi_i}{d\eta}\frac{d\psi_j}{d\eta}d\eta - \frac{Ha^2\cos^2\theta}{(1+Nh^2)}\int_{\eta_e}^{\eta_{e+1}} \psi_i\psi_j d\eta - \frac{1}{Da}\int_{\eta_e}^{\eta_{e+1}} \psi_i\psi_j d\eta \\
& - \frac{Fs\bar{u}_1}{Da}\int_{\eta_e}^{\eta_{e+1}} \psi_i\psi_1\psi_j d\eta - \frac{Fs\bar{u}_2}{Da}\int_{\eta_e}^{\eta_{e+1}} \psi_i\psi_2\psi_j d\eta, \\
K_{ij}^{12} =& \frac{2}{Ek}\int_{\eta_e}^{\eta_{e+1}} \psi_i\psi_j d\eta + \frac{Ha^2Nh\cos\theta}{(1+Nh^2)}\int_{\eta_e}^{\eta_{e+1}} \psi_i\psi_j d\eta, \\
K_{ij}^{21} =& -\frac{Ha^2Nh\cos\theta}{(1+Nh^2)}\int_{\eta_e}^{\eta_{e+1}} \psi_i\psi_j d\eta - \frac{2}{Ek}\int_{\eta_e}^{\eta_{e+1}} \psi_i\psi_j d\eta, \\
K_{ij}^{22} =& -\int_{\eta_e}^{\eta_{e+1}} \frac{d\psi_i}{d\eta}\frac{d\psi_j}{d\eta}d\eta - \frac{Ha^2}{(1+Nh^2)}\int_{\eta_e}^{\eta_{e+1}} \psi_i\psi_j d\eta - \frac{1}{Da}\int_{\eta_e}^{\eta_{e+1}} \psi_i\psi_j d\eta \\
& - \frac{Fs\,\bar{v}_1}{Da}\int_{\eta_e}^{\eta_{e+1}} \psi_i\psi_1\psi_j d\eta - \frac{Fs\,\bar{v}_2}{Da}\int_{\eta_e}^{\eta_{e+1}} \psi_i\psi_2\psi_j d\eta
\end{aligned}
\tag{40}
$$

and

$$
b_i^1 = -\left(\psi_i\frac{du}{d\eta}\right)_{\eta_e}^{\eta_{e+1}} - Np\int_{\eta_e}^{\eta_{e+1}} \psi_i\, d\eta, \qquad b_i^2 = -\left(\psi_i\frac{dv}{d\eta}\right)_{\eta_e}^{\eta_{e+1}}, \tag{41}
$$

where

$$
\bar{u} = \sum_{i=1}^{2} \bar{u}_i\psi_i, \qquad \bar{v} = \sum_{i=1}^{2} \bar{v}_i\psi_i. \tag{42}
$$

Each element matrix is of the order 4×4. Since the whole domain is divided into a set of 160 line elements, therefore following assembly of all the elements equations we obtain a matrix of order 322×322. This system of equations is non-linear therefore an iterative scheme has been used to solve it. The system is linearized by incorporating the functions $\bar{u}\,and\,\bar{v}$, which are assumed to be known. After applying the given boundary conditions only a system of 318 equations remains for solution which is achieved using Gauss elimination method maintaining an accuracy of 0.0005. Benchmarking of the source FEM code has been performed against finite difference methods. Excellent agreement

was found. Details have been omitted however for brevity. The *line elements* employed achieved *rapid convergence*. A *monotonic* convergence criterion was also established for which the 2-node line elements employed were selected to ensure that the mesh was compatible. When monotonic convergence is achieved the accuracy of the solution results in a *continuous increase* with further refinement of the finite element mesh. As such mesh refinement is executed by delineating *a priori* utilized elements into two or more elements, resulting in "embedding" in the new mesh. Effectively, as documented by Bathe [49] the *new space* of finite element interpolation functions encapsulates the *previously utilized space* and, with mesh refinement, the dimension of the finite element solution space is *enhanced continuously* to embody the exact solution.

6 Results and discussion

In the present study we examine the influence of Hartmann number (Ha), Hall current parameter (Nh), Darcy number (Da), Forchheimer number (Fs), Ekman number (Ek), dimensionless pressure gradient parameter (Np), and orientation of the applied magnetic field (θ) on *u, v and shear stresses at the plate*, with separation of the plates (η). Representative values are used to simulate physically realistic flows. Throughout we have adopted $Da = 0.1$, $Ek = 0.25$, $Nh = 0.5$, $Fs = 1$, $Ha = 3$, $Np = 0.5$ and $\theta = \pi/4$ unless otherwise indicated. Such data constitute a *weakly rotating magnetohydrodynamic flow with Hall currents flowing through a weakly non-Darcian regime under weak constant pressure gradient, with the magnetic field inclined at 45 degrees to the positive y-axis (axis of rotation).*

In **figure 2** we have computed the distribution of primary flow velocity, u, versus the transformed coordinate, η, for the purely fluid regime scenario i.e. for Da $\rightarrow \infty$ and Fs = 0. Under these conditions, the governing equations reduce to Case V i.e. the non-porous case examined by Ghosh and Pop [36]. Excellent agreement for all inclinations of the magnetic field i.e. all θ values are seen. With increasing orientation from $\pi/3$ i.e. 60 degrees to $\pi/2$ i.e. 90 degrees, we observe that the primary velocity, u, is increased. However as θ is increased to greater than 90 degrees i.e. when the orientation becomes obtuse, clearly the velocity u is also decreased. The minimal velocity corresponds to $\theta = \pi$ for which the magnetic field has swept through to the opposite direction with respect to the rotation axis i.e. instead of being orientated to the positive y axis, it is now in fact directed along the negative y axis. From this we can infer that the best control mechanism for the flow velocity in a variable angle magnetohydrodynamic generator, would correspond to the negative y axis i.e.

maximum retardation would be achieved for this scenario. In consistency with classical MHD channel flow, all profiles are symmetrical parabolas about the centre line of the channel i.e. about η =0. We note that the *Ek* parameter defines the ratio of the hydrodynamic viscous force to the Coriolis (rotational) force. As such the value Ek = 0.25 corresponds to a weak rotation of the flow. For Ek $\sim$ 1 in a rotating fluid near a flat plate the Ekman boundary layer is generated where the viscous and Coriolis forces are of the same order of magnitude. For the present case of fully developed flow we do not consider boundary-layer regimes. The pressure gradient parameter for figure 2 (and **figure 3**) is also held constant at unity and intermediate magnetic field is imposed (Ha $\sim$ 3.162) for which Hall currents are ignored (Nh =0). It is also worth noting that, as with Ghosh and Pop [36] the velocity distribution is identical when $\theta = \eta\pi$ and (2n +1) $\pi/2$.

A similar trend is observed for the development of the secondary velocity profile, v, with η coordinate across the rotating channel, except that the velocity is always negative indicating that *backflow* dominates in the secondary flow field. We observe that the magnitude of v increases with increasing orientation from $\pi/4$ i.e. 45 degrees to $\pi/3$ i.e. 60 degrees, and thence to $\pi/2$ i.e. 90 degrees. However as with primary flow velocity, when θ is increased to greater than 90 degrees i.e. π for which the magnetic field has swept through to the opposite direction with respect to the rotation axis i.e. instead of being orientated to the positive y axis, the secondary velocity magnitude is infact decreased. Once again the computations show excellent agreement with the analytical solution of Ghosh and Pop [36].

In **figures 4a and 4b** we have illustrated the variation of primary and secondary velocity with the *Darcy number (Da).* A substantial increase in primary velocity, u, is observed as Da increases from 0.01 (low permeability regime) to 0.1 and then to 1 (high permeability). In the momentum equation (24), the Darcian bulk impedance term, $-\frac{u}{Da}$ is inversely proportional to the Da parameter. The FEM computations are shown in figure 4a. The Darcy drag force arises from the viscous contribution to stress at the solid particle boundaries. As such with increasing permeability (and Da value) the flow receives progressively less resistance from the porous fibers which diminish in concentration. Consequently flow is accelerated with a rise in Da and primary velocities increased. An interesting feature of the profiles for all Da values is that they are flattened near the centre of the channel. The extent of the flattened central zone in the graphs is increased for lower Da values. For all three profiles there is a sharp descent from the plateau to zero at each of the plates (no-slip condition at the channel boundaries). In figure 4b, the secondary velocity distribution, $v$is shown. In this case, again an increase in Da serves to boost the velocity considerably. For very low Da values (0.01) the secondary velocity diminishes to near zero in value.

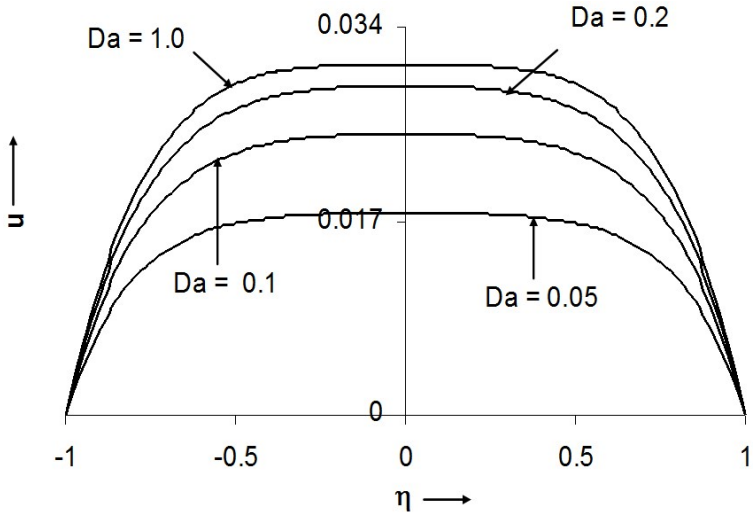

(a) Variation of u

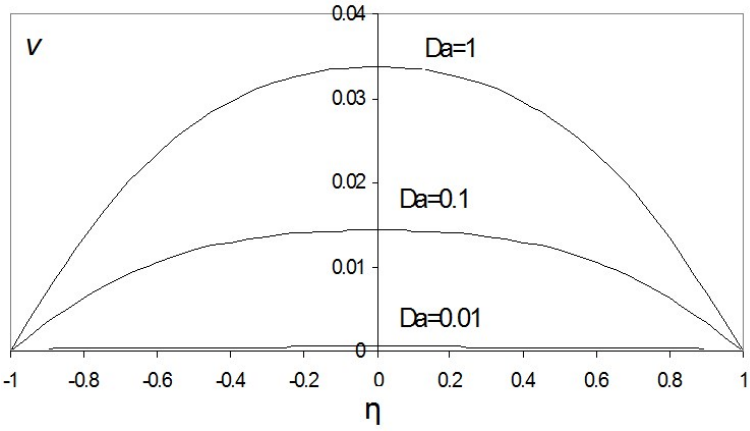

(b) Variation of v

Figure 4: Variation of u and v with η for various Da[0.001, 0.01, 0.1, 1] for Ha = 3, Nh = 0.5, Fs = 1, Ek = 0.25, Np = 0.5, $\vartheta = \pi/4$. **(FEM)**

This is contrary to the primary flow velocity, u, which remains non-trivial even at the lowest Da value (figure 4a). Secondary flow is therefore more strongly affected by permeability changes than the primary flow. All profiles resemble the classical Hartmann channel flow parabolic profiles, but are considerably more curved than for the primary velocity distribution, u.

Figures 5a and **5b** illustrate the influence of *Forchheimer number* (Fs) on primary and secondary velocity profiles. A decrease in Fs from 25 through 10, 5,

2, 1 to 0.1,causes a considerable increase in primary velocity. In the primary flow momentum equation (24), inertial effects due to the porous medium are experienced via the final term on the right hand side, $-\frac{Fs}{Da}u^2$. The Forchheimer drag term does not explicitly involve viscosity but does arise from viscosity action, mediated by the inertial effects affecting the distribution of pressure which also contributes to the stress at the solid boundaries (plates) in the regime. Forchheimer dragmodels essentially a "form drag phenomenon", and infact involves the separation of boundary layers and wake formation behind solid obstacles.

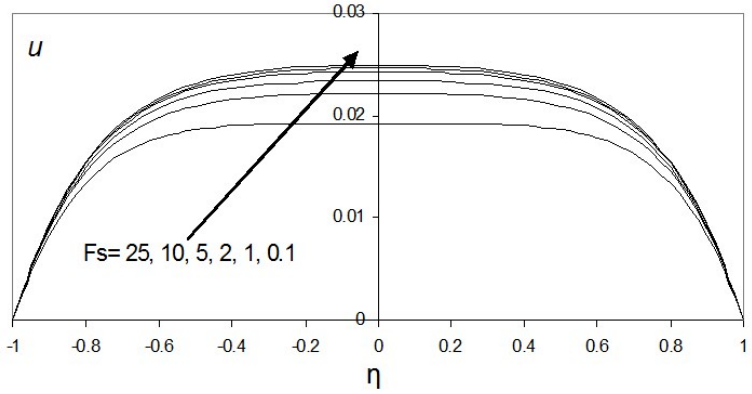

(a) Variation of u

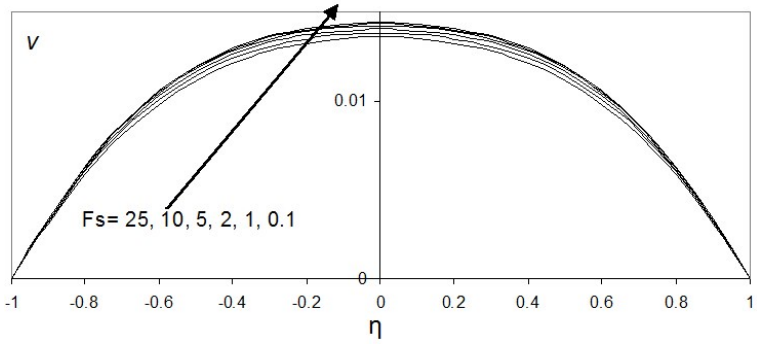

(b) Variation of v

Figure 5: Variation of u and v with η for various Fs[0.1, 1, 2, 5, 10, 25] for Ha = 3, Nh = 0.5, Da = 0.1, Ek = 0.25, Np = 0.5, $\vartheta = \pi/4$. **(NSM Method)**

The pore scale convective inertial effects contributing to the form drag lead to a substantial alteration of the velocity field and exacerbate the macroscopic region in which the pore scale velocity gradients are large. These characteristics apply to both porous media of the bluff body type as well as those of the conduit

type (relevant to the present paper). Forchheimer drag simulates the strong inertial flow regime in porous media hydrodynamics. This pertains to the regime where the pore Reynolds number, Re_p based on a consideration of the particle or pore diameter, is greater than or equal to unity. At this point the model departs from the purely *Darcian or viscous-dominated* classical porous media transport physics. Profiles for primary flow are seen to be relatively flattened between -0.8 ¡ η ¡ 0.8, and then decay sharply to zero at the channel plate boundaries ($\eta = \pm$ 1). In figure 5b, secondary velocity, v, which is affected via the secondary Forchheimer drag term in equation (25), $-\frac{Fs}{Da}v^2$, is seen to increase with a decrease in Fs. However the changes are much less dramatic than in the case of the primary flow velocity distribution (figure 5a). Profiles are also much more parabolic in nature with an absence of flatness near the centre of the channel. Forchheimer drag therefore has much less effect on secondary velocity and none at all in the near-plate regions ($\eta < -0.85$ and $\eta > 0.85$).

The influence of hydro-magnetic parameter, the *Hartmann number, Ha* on u and v distributions is depicted in **figures 6a** and **6b**. An increase in Ha from 1 (where *Lorentz hydro-magnetic drag is of the same order as the viscous force in the flow*) to 3, 5, and 10 induces a significant decrease in primary velocity across the channel. Profiles are symmetric and plateau-like across most of the channel width (- 0.8 $\leq \quad \eta \quad \leq$ 0.8). Secondary velocity profiles are also decreased with a rise in Ha, and more so than in the case of primary flow velocity. In the secondary momentum equation, the hydro-magnetic drag (albeit modified for Hall current and oblique magnetic field effects), $-\frac{Ha^2}{1+Nh^2}[v + Nhu\cos\theta]$**,** remains negative i.e. impedes the flow development, resulting in more dramatic reduction in the secondary field flow.

In figures **7a** and **7b**, the influence of *Hall parameter, Nh*, on *u and v* distributions across the channel are given. The presence of a Hall current in the flow causes two-dimensionality. Longitudinal Hall current imparts a transverse body force which in turn generates transverse gradient in velocity. Primary velocity in the channel is seen to decrease with an increase in *Nh* values from 0 (no Hall current), through 0.2, 0.5, 1.0 to 1.5. A similar behaviour was reported by Ghosh and Pop [36]. We infer from the primary momentum equation (24) that the *Nh parameter* is expressed in the reciprocal – the primary flow velocity term with Hall current will then be $-\frac{Ha^2\cos\theta}{1+Nh^2}u\cos\theta$ **i.e.** $-\frac{Ha^2\cos^2\theta}{1+Nh^2}u$. An increase in Nh will induce for small Nh values very minor alterations in the expression *1* $+Nh^2$. However in the secondary momentum equation, the term, $-\frac{Ha^2}{1+Nh^2}[v + Nhu\cos\theta]$, gives an effective contribution to primary velocity field, u, of $-\frac{Ha^2}{1+Nh^2}Nhu\cos\theta$ i.e. $-\frac{NhHa^2Cos\theta}{1+Nh^2}u$ indicating that an increase in Nh causes a direct increase in the *drag force* term affecting the primary velocity, u.

This secondary effect is the principal reason explaining the decrease in primary flow velocity with an increase in Hall current parameter, Nh which effectively *decelerates* the flow.

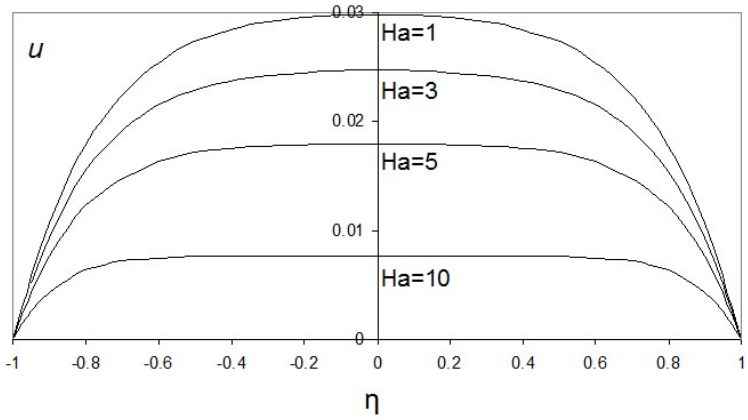

(a) Variation of u

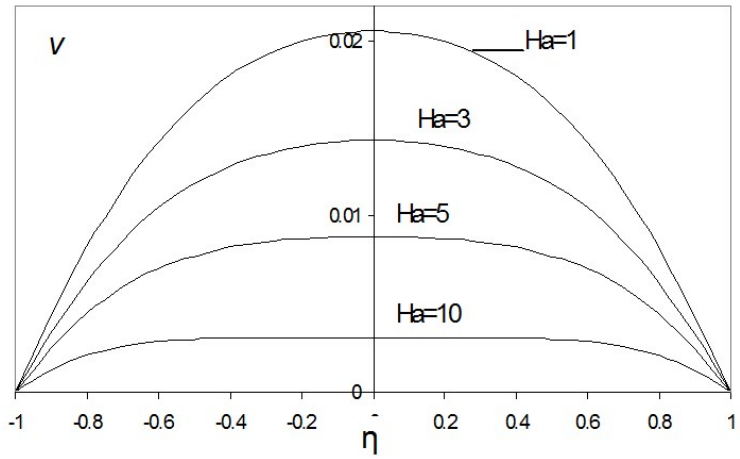

(b) Variation of v

Figure 6: Variation of u and v with η for various Ha $\in [1, 3, 5, 10]$ for Nh = 0.5, Da = 0.1, Fs = 1, Ek = 0.25, Np = 0.5, $\vartheta = \pi/4$. **(NSM Method)**

Conversely we observe that the secondary velocity, v, is in fact increased with a rise in Hall current parameter, Nh. Peak values (at the channel centre line, η =0) rise from 0.011 to 0.019 as Nh increases from 0 (Hall effect neglected) through 0.5, 1.0 to 1.5. A similar argument applies here. In the secondary momentum equation a change in Nh has very little effect, due to the

inverse relationship on the secondary velocity, v for Nh ¡ 1 [it is affected via the term $-\frac{Ha^2}{1+Nh^2}v$]. This effect will impede the secondary flow. However it will be swamped out by the much greater direct proportionality in the factor affecting the secondary velocity in the primary momentum equation, viz $\frac{NhHa^2Cos\theta}{1+Nh^2}v$. This positive term accelerates the flow for increase in Nh, explaining the rise in secondary flow velocity, v, with increase in Nh in figure 7b. The mechanism by which Hall currents influence hydro-magnetic channel flow (whether translational or rotational) is therefore via *secondary* effects and coupling in the momentum equations.

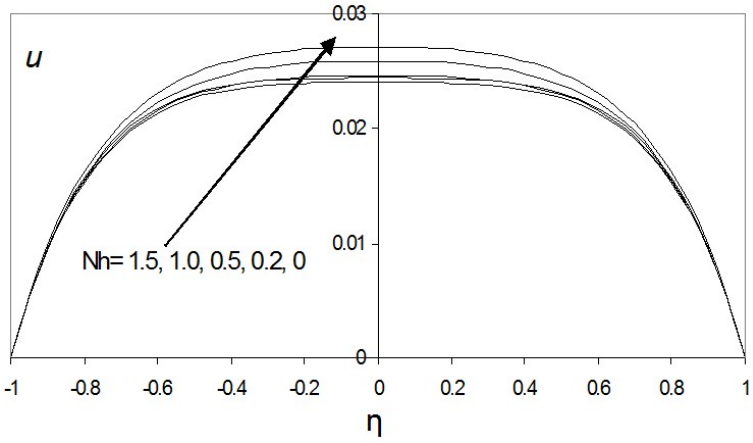

(a) Variation of u

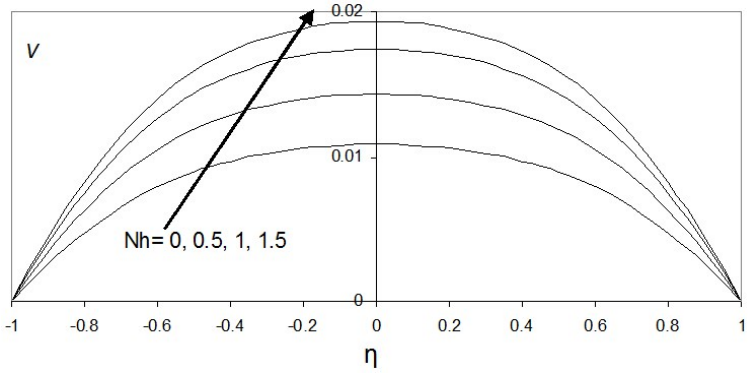

(b) Variation of v

Figure 7: Variation of u and v with η for various Nh $\in [0.0, 0.5, 1.0, 1.5]$ for Ha = 3, Da = 0.1, Fs = 1, Ek = 0.25, Np = 0.5, $\vartheta = \pi/4$. **(NSM Method)**

Figures 8a and **8b** show the effect of the *rotational parameter, Ek*, on

primary and secondary velocity components across the channel. Primary velocity u is seen to decrease substantially as Ek decreases from 1 through 0.5, 0.25 to 0.1. Ek represents the relative contribution of viscous and rotational forces. *Smaller Ek values imply greater rotational effects.* The viscous and rotational forces are of the same order of magnitude for Ek = 1. Primary velocity is affected via the secondary momentum equation coupling, through the term $2\frac{u}{Ek}$.

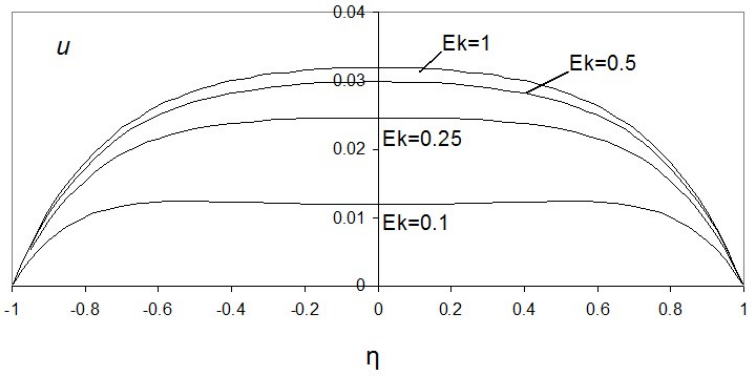

(a) Variation of u

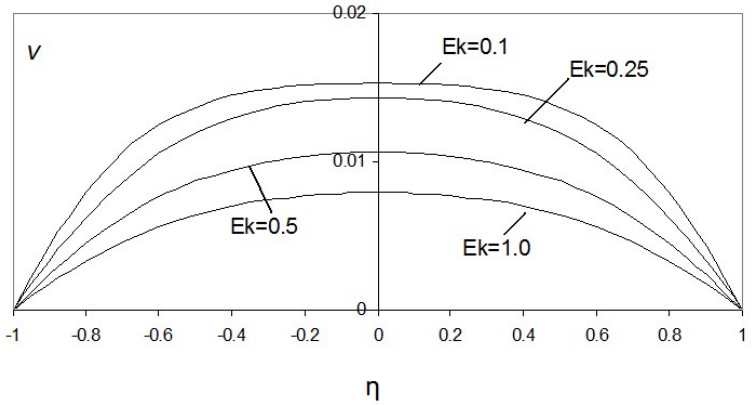

(b) Variation of v

Figure 8: Variation of u and v with η for various Ek $\in [0.1, 0.25, 0.5, 1.0, 2.0, 5.0]$ for Ha = 3, Nh = 0.5, Da = 0.1, Fs = 1, Np = 0.5, $\vartheta = \pi/4$. **(NSM Method)**

This is in fact a drag force (it becomes negative when migrated to the right hand side of (25). As such increasing Ek will decrease the drag force (inverse proportionality) and this will serve to accelerate the primary velocity field i.e. increase u values with greater Ek values. The converse is apparent for the

secondary velocity distribution, v, which is controlled by the coupling term in the primary momentum equation (24), viz, $-2\frac{v}{Ek}$, which becomes positive when migrated to the right hand side of (24). As such this force is a positive body force which serves to accelerate the flow. However as Ek increases the magnitude of this force of course decreases explaining the plummet in secondary velocity, v with a rise in Ek in figure 8b. Although we have studied only low Ek number effects in the present analysis, the case of maximum Ek value i.e. 1 in this paper, is important. It corresponds to the formation of an Ekman boundary layer in the plate vicinity. The system is a relatively strong rotating system in this scenario. As will be seen later, for low Ek values the magnetic field has greater influence on the dynamics of plasma flow, as indicated by Nanda and Mohanty [23]. Unfortunately in that study only extreme cases of Ek have been considered, for which analytical solutions are possible. A primary objective of the present study has been to widen the sensitivity of the analysis to various low Ek values, to ascertain exactly how plasma rotating channel flow responds to strong rotational effects.

The influence of pressure gradient parameter, Np, on u and v velocity component distributions is shown in **figures 9a** and **9b**. Ghosh and Pop [36] studied only the case of Np = 1. As such there is no data in their study elucidating how an increase or decrease in dimensionless pressure gradient affects the flow. We observe in figure 9a that an increase in Np accelerates the primary flow i.e. increases the u values considerably. Maximum central channel u value rises from about 0.005 for Np = 0.1 to 0.049 for Np = 1 an increase of almost 1000 % (a tenfold increase). Np appears only in the primary momentum equation, where clearly it is a positive body force and will enhance flow velocities. This is of significance in plasma MHD energy systems where it is evident that higher momentum can be achieved simply by increasing pressure gradient in the x-direction. Via coupling with the secondary flow equation (25) we observe that secondary velocity, v, is also increased with a rise in Np, but for the same increase in Np (from 0.1 to 1) the escalation in v values is less i.e. from 0.005 to 0.028 constituting a 500 % increase. For small Ek values (i.e. 0.25 for figures 9a and 9b), the Taylor-Proudman theorem shows that the influence of pressure gradient will be *two-dimensiona*l, especially in the core of the channel (around the centre-line), which indeed is consistent with the present computations.

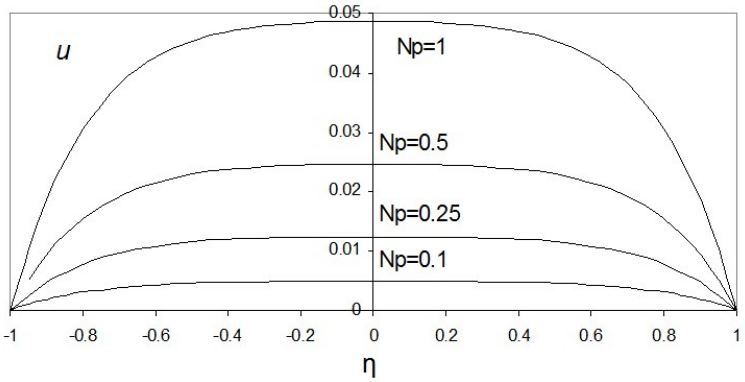

(a) Variation of u

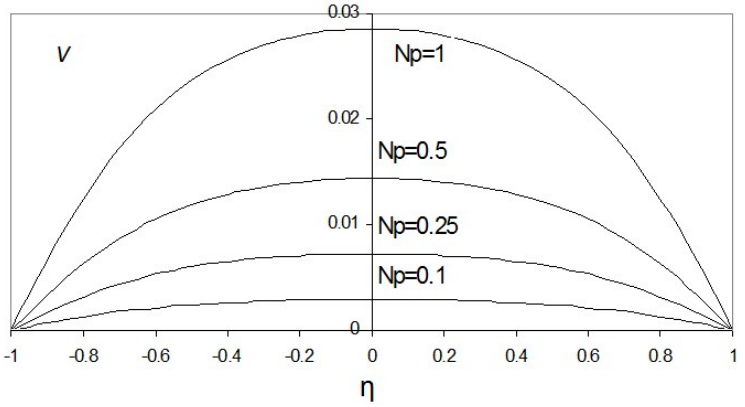

(b) Variation of v

Figure 9: Variation of u and v with η for various Np $\in [0.1, 0.25, 0.5, 1.0]$ for Ha = 3, Nh = 0.5, Da = 0.1, Fs = 1, Ek = 0.25, $\vartheta = \pi/4$. **(NSM Method)**

Profiles of *u and v versus* η for various orientations of the magnetic field, θ, are depicted in **figures 10a, b**. We observe that as θ increases from 0 to $\pi/4$ u value decreases. In the primary momentum equation, the influence of θ is experienced via the $\frac{Ha^2 \cos\theta}{1+Nh^2}[-u\cos\theta]$ term which simplifies to $-\frac{Ha^2 \cos^2\theta}{1+Nh^2}u$. This is adrag force term, implying that a rise in the value of Cos θ will increase impedance to the primary flow and cause a deceleration. Cos θ values decrease from 1 for $\theta = 0$ (where the magnetic field, B_o is directed along the rotation axis i.e. y-axis) to 0.707 for $\theta = \pi/4$; the *value of* $Cos^2\theta$ *will change from 1 to 0.5* and the drag force therefore *decreases* as θ increases from 0 to $\theta = \pi/4$, explaining the increase in u value. Incidentally the u value will be the same for $\theta = 0$, π and 2π i.e. the same magnetic drag force will be experienced by the

fluid when the field is inclined along the y axis or the negative y axis direction. As θ increases to $\pi/3$, $5\pi/6$ and then falls to $\pi/2$, the value of Cos θ changes from 0.5 to -0.866 and then to 0. As a result the value of $\mathrm{Cos}^2\theta$ will become *0.25, 0.75 and then to 0,* respectively. Hydromagnetic drag force, $-\frac{Ha^2\cos^2\theta}{1+Nh^2}u$, for constant Ha and Nh (which are prescribed values of 3 and 0.5 respectively), will respectively *decrease* from $\theta = \pi/4$ (for which $\mathrm{Cos}^2\theta = 0.5$] to the new value for $\theta = \pi/3$ ($\mathrm{Cos}^2\theta = 0.25$), then increase for $\theta = 5\pi/6$ ($\mathrm{Cos}^2\theta = 0.75$), and then fall to 0. Hence the minimum hydro-magnetic drag force will correspond to the last of these cases i.e. $\theta = \pi/2$, for which there will be no hydro-magnetic drag, explaining the maximum primary velocity for this case. In MHD plasma generator design, therefore the highest velocity for a given magnetic field strength will be achieved for a magnetic field imposed at 90 degrees ($\theta = \pi/2$) to the y-axis (rotation axis). In nuclear fusion control problems, the minimum primary flow velocity will be of importance and this will be achieved for the maximum hydro-magnetic drag i.e. for the maximum value of $\mathrm{Cos}^2\theta$, which is associated with the case $\theta = 0$ i.e. where the magnetic field, B_o is directed along the rotational (y) axis. Let us now consider the influence of θ on secondary flow velocity. In equation (25), the hydro-magnetic drag force term (containing θ contribution) takes the form, $-\frac{Ha^2}{1+Nh^2}[v + Nhu\cos\theta]$, where we immediately observe two important facts- firstly that θ appears in Cosθ (and not $\mathrm{Cos}^2\theta$, as with the primary flow equation (24)) and secondly that Cosθ is coupled to the primary velocity, u, not the secondary velocity, v. The influence of changing Cos θ will therefore be experienced indirectly by the secondary velocity and we expect a different change over the same variation of θ. This is indeed the case in figure 10b where we observe that the difference in centerline peak values of v is 0.05 (minimum) to 0.15 (maximum). Over the same effective range of θ (i.e. from 0 to π) we observe in figure 10a that the primary velocity changes at $\eta = 0$ from 0.025 to 0.035, although of course these values correspond to different values of θ in both cases.

As θ changes from $\pi/2$, $\pi/3$, $\pi/4$, 0 and 2π, to $5\pi/6$ and finally to π, Cos θ changes in value from 0, 0.5, to 0.707, to 1 (maximum), -0.87 and then to -1. As a result the hydro-magnetic drag will increase for the first three of these values and then infact become positive for the last two. Progressively therefore the flow will be accelerated i.e. the maximum velocities should correspond to $\theta = \pi$. This is indeed indicated on figure 10b.

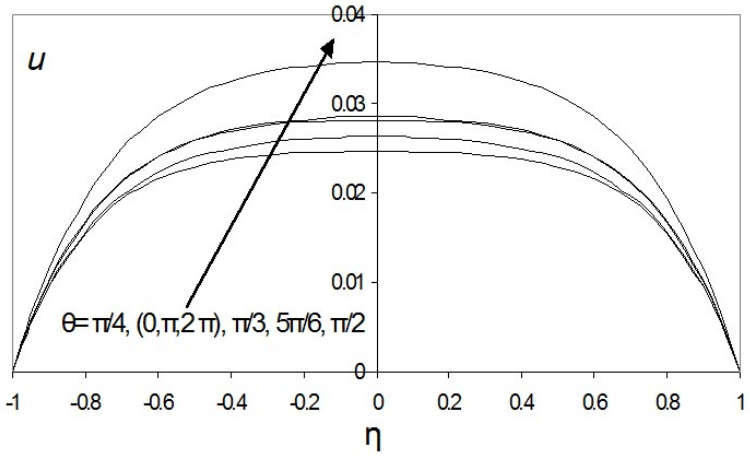

(a) Variation of u

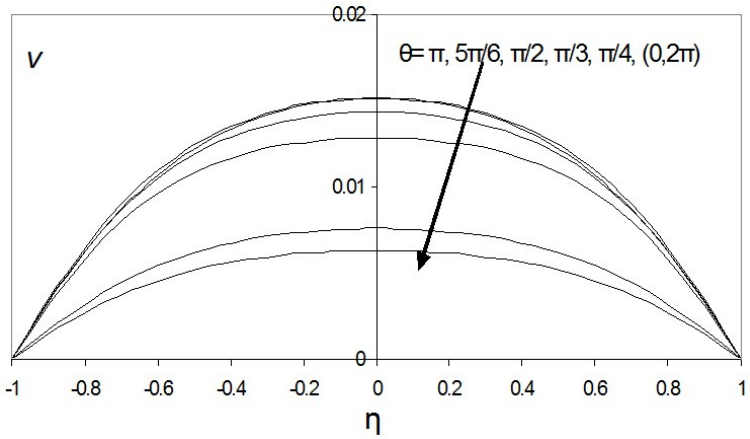

(b) Variation of v

Figure 10: Variation of u and v with η for various $\vartheta \in [0, \pi/4, \pi/3, \pi/2, 5\pi/6, \pi, 2\pi]$ for Ha = 3, Nh = 0.5, Da = 0.1, Fs = 1, Np = 0.5, Ek = 0.25. **(NSM Method)**

We have also computed, using FEM, the variation of shear stresses at the lower plate due to the primary and secondary velocity fields for the effects of *Da, Fs, Nh and* θ are shown in **figures 11** to **14**.

We observe in **figure 11** that as Da increases from 0.1 to unity (very high permeability) primary shear stress at the lower plate (τ_u at η = -1) is *increased* in magnitude since the Darcian drag force is reduced with a rise in Da; while magnitude of the secondary shear stress at the lower plate (τ_v at η = -1) is also

increased, values become more negative with a rise in Da, indicating significant *backflow*. However flow separation does not occur as shear stresses are never zero, a result consistent with the deductions of Nanda and Mohanty [23] among other researchers.

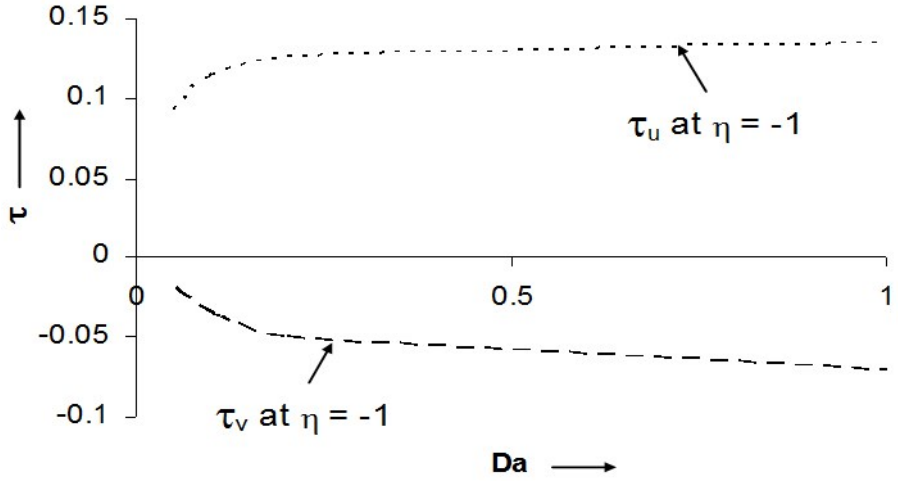

Figure 11: Shear stress τ for various Darcy numbers (Da) values at the lower plate **(FEM solution)**

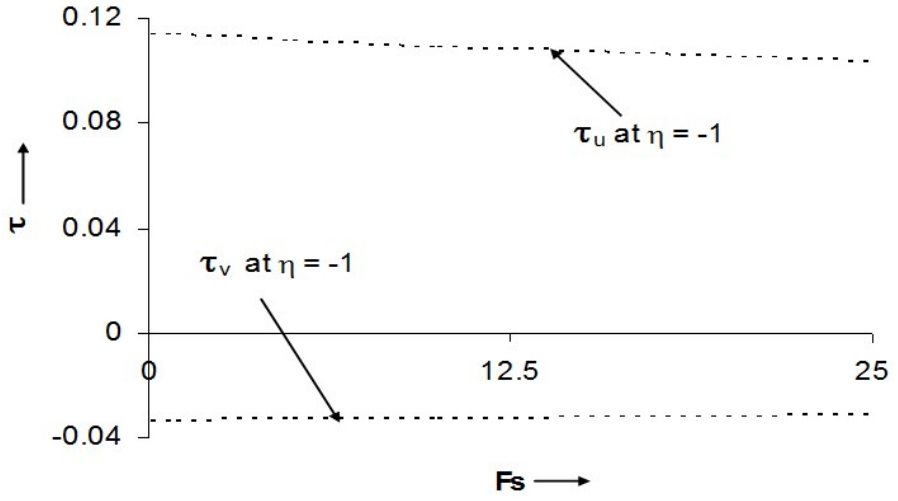

Figure 12: Shear stress τ at various Fs values at the lower plate **(FEM solution)**

Conversely, **figure 12** indicates that as *Forchheimer number, Fs* is increased from 0.1 to 25, corresponding to a significant increase in inertial (quadratic porous resistance) primary shear stress at the lower plate (τ_u at η = -1) is *decreased* in magnitude. Very little difference however in secondary shear stress at the lower plate (τ_v at η = -1) is observed, since magnitudes of secondary velocity are substantially lower than the primary velocity. As such the secondary Forchheimer drag force will have very small values as it is a function of the secondary velocity, v.

The influence of *Hall current parameter, Nh*, is shown in **figure 13**, from which we deduce that primary shear stress at the lower plate (τ_u at η = -1) is initially decreased slightly but with larger Nh values is slightly enhanced. There is a larger decrease in secondary shear stress at the lower plate (τ_v at η = -1) with increasing Nh values, initially; however with subsequent increase the profile stabilizes.

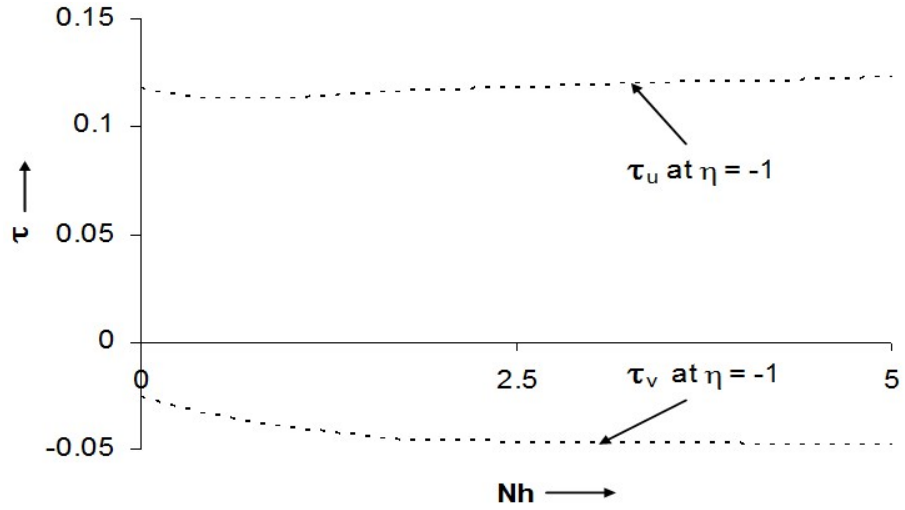

Figure 13: Shear stress τ at various Nh values at the lower plate**(FEM solution)**

Finally in **figure 14**, the effect of magnetic field inclination, θ on the shear stress values indicates that primary shear stress at the lower plate (τ_u at η = -1) is increased steadily with increasing values of θ (plotted in radians) i.e. the primary flow at the lower channel plate is accelerated. There is a slight decrease in secondary shear stress at the lower plate (τ_v at η = -1) with initial increase in θ, but generally very little effect on the secondary flow shear stress at the channel lower plate is observed.

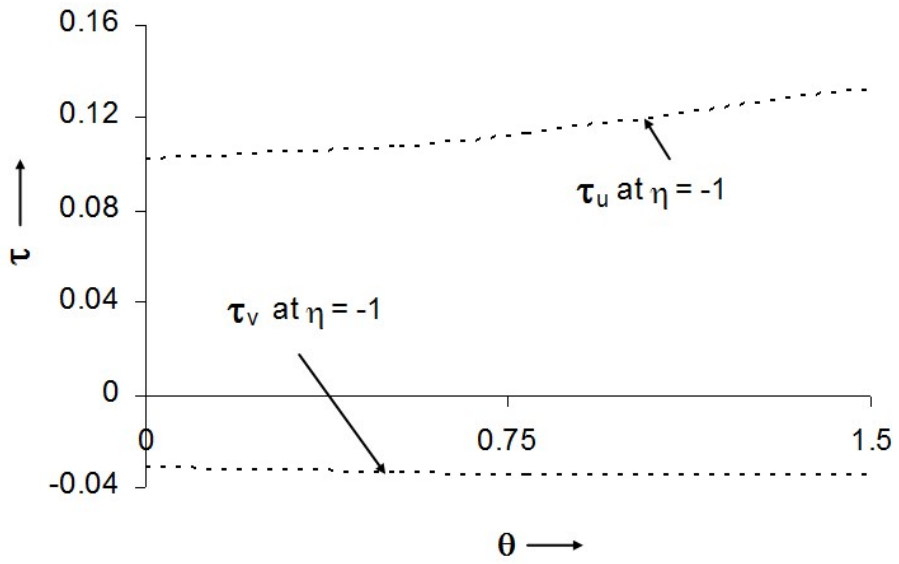

Figure 14: Shear stress τ at various θ values at the lower plate **(FEM solution)**

7 Conclusions

We have described in detail a new theoretical model for rotating hydro-magnetic flow in a nonlinear, isotropic, homogenous porous medium channel system in the presence of Hall currents, under the action of an inclined magnetic field and a unidirectional pressure gradient. The general equations for rotating magnetoplasma dynamics have been reduced to a set of *viscous hydro-magnetic partial differential equations* which have been transformed to a pair of nonlinear ordinary differential equations under appropriate boundary conditions. These primary and secondary momentum equations are shown to be dictated by the Hartmann number (Ha), Hall current parameter (Nh), Darcy number (Da), Forchheimer number (Fs), Ekman number (Ek) and dimensionless pressure gradient parameter (Np) and also the orientation of the applied magnetic field (θ). A number of special cases are derived. The succinct aspects of network simulation method used to solve the transformed two-point boundary value problem, are discussed. A finite element solution is also developed. The present study has shown that both primary and secondary flow fields are accelerated with increasing Darcy number, increasing Forchheimer number and increasing pressure gradient parameter. They are however decelerated with a rise in Hartmann (hydro-magnetic) number. Primary velocity, u is decreased with increasing Hall current parameter (Nh) whereas secondary velocity, v, is conversely increased. Primary velocity is however increased

with a rise in rotational parameter, Ek i.e. Ekman number, (corresponding to a decrease in rotational effects) whereas the secondary velocity is decreased with a rise in Ek. A thorough explanation is provided for this behaviour. Primary velocity is seen to increase for certain orientations of the magnetic field and these are discussed with pertinence to MHD energy generators. The important stabilizing influence of a porous medium has been demonstrated in the present study; porous media therefore hold excellent potential for controlling rotating hydro-magnetic flows in MPD (Magneto-Plasma Dynamic) thruster systems.

References

[1] Osmond, L., *Electromagnetic Propulsion*, BSc Final Year Project, Aerospace Technology, Sheffield Hallam University, May (2011).

[2] Womac, G.J., MHD Power Generation, Chapman and Hall, London (1969).

[3] Rosa, R.J., Magnetohydrodynamic Energy Conversion, Hemisphere Publishing, Washington D.C. (1987).

[4] Heiermann, J. and M. Auweter-Kurtz, Numerical investigation of the electrodes in high power self- field MPD thrusters (work at the Institut fuer Raumfahrtsysteme, Stuttgart, Germany), AIAA-2002-2102, *Electrical Propulsion session I,*33^{rd} Plasmadynamics and Lasers Conference & 14^{th} International Conference on MHD Power Generation and High Temperature Technologies, 20 - 23 May, Westin Maui Maui, Hawaii, USA (2002).

[5] Sutton, G.W. and Sherman, A. Engineering Magnetohydrodynamics, MacGraw-Hill, New York (1965)

[6] Inui, Y.,Ishikawa, Ishikawa, M. and Omoto, J., New conceptual design method for non-equilibrium disk MHD generator, Energy Conversion and Management, 36, 109-119 (1995).

[7] Al-Nimr, M. A. MHD free-convection flow in open-ended vertical concentric porous annuli, Applied Energy, 50, 4, 293-311 (1995).

[8] Chatuverdi, N., On MHD flow past an infinite porous plate with variable suction, Energy Conversion and Management, 37, 623-627 (1996).

[9] Inoue, I., Lineberry, J.T., Ishikawa, M. and Umoto, J., Numerical study of the electrodynamics behaviour of the CDIF MHD generator, Energy Conversion and Management, 39, 785-795 (1998).

[10] Chen, L., Gong, J., Sun, F. and Wu, C., Heat transfer effect on the performance of MHD power plant, Energy Conversion and Management, 43, 2085-2095 (2002).

[11] Ishikawa, M., Koshiba, Y. and Matsushita, T., Effects of induced magnetic field on large scale pulsed MHD generator with two phase flow, Energy Conversion and Management, 45, 707-724 (2004).

[12] Aïboud-Saouli, S., N. Settou, S. Saouli, N. Meza Second-law analysis of laminar fluid flow in a heated channel with hydro-magnetic and viscous dissipation effects, Applied Energy, 84, 3, 279-289 (2007).

[13] Sato, H., The Hall effect in viscous flow of ionized gas between two parallel plates under transverse magnetic field, J. Physical Society (Japan), 16, 1427 (1961).

[14] Yamanishi, T., Hall effect in the viscous flow of ionized gas through straight channels, 17^{th} Annual Meeting, Physical Society of Japan, 5, 29 (1962).

[15] Katagiri, M., The effect of Hall currents on the viscous magnetohydrodynamic boundary layer flow past a semi-infinite flat plate, J. Physical Society (Japan), 27, 1051 (1969).

[16] Pop, I. and Soundalgekar, V.M., Effects of Hall current on hydro-magnetic flow near a porous plate, Acta Mechanica, 20, 315-318 (1974).

[17] Gupta, A.S., Hydrodynamic flow past a porous flat plate with Hall effects, Acta Mechanica, 22, 281 (1975).

[18] Masapati, G.H., Mittal, M.L. and Rao, B.N., Entrance flow in a MHD channel with Hall and ionslip currents, AIAA J., 14,1768-1770 (1976).

[19] Bhat, A.N. and Mittal, M.L., Effect of Hall and ionslip currents in heat transfer with uniform wall heat flux in the developing flow region, Mechanics Research Communications, 5, 121-126 (1978).

[20] Soundalgekar, V.M., Vighnesam, N.V. and Takhar, H.S.: Hall and ion-slip effects in the MHD Couette flow with heat transfer. IEEE Trans. Plasma Science. 7,178-182, (1979).

[21] Singh, A. K., Hall effects on the oscillatory MHD flow in the Stokes problem past an infinite vertical porous plate. II. Astrophysics and Space Science J. 97, 2, 453-460 (1983).

[22] Kinyanjui, M., Kwanzi, J.K. and Uppal, S.M., Magnetohydrodynamic free convection heat and mass transfer of a heat generating fluid past an impulsively started infinite vertical porous plate with Hall current and radiation absorption, Energy Conversion and Management, 42, 917-931 (2001).

[23] Nanda, R.S. and Mohanty, H.K., Hydromagnetic flow in a rotating channel, Appl. Sci. Res., 24, 65-78 (1970).

[24] Soundalgekar, V. M. and J. P. Bhat, MHD flow and heat transfers in a viscous electrically conducting fluid in a rotating channel between conducting plates
Applied Energy, 20, 141-151 (1985).

[25] Arikoglu, A., Ozkol, I. and Komurgoz, G., Effect of slip on entropy generation in a single rotating disk in MHD flow, Applied Energy, 85, 1225-1236 (2008).

[26] Bég, O. Anwar H. S. Takhar, G. Nath and A. J. Chamkha, Mathematical Modeling of hydro-magnetic convection from a rotating sphere with impulsive motion and buoyancy effects, Non-Linear Analysis: Modeling and Control, 11, 3, 227-245 (2006).

[27] S.K. Ghosh, O. Anwar Bég and J. Zueco, Rotating hydro-magnetic optically-thin gray gas flow with thermal radiation effects, J. Theoretical Applied Mechanics. 39, 1, 101-120 (2009).

[28] Takhar, H.S., Ram, P.C., and Singh, S.S. Unsteady MHD flow of a dusty viscous liquid in a rotating channel with Hall currents, Int. J. Energy Research, 17, 69-74 (1993).

[29] T. Miyoshi and K. Kusano, MHD simulation of a rapidly rotating magnetosphere interacting with the external plasma flow, Geophysical Research Letters, 24, 21, 2627-2630 (1997).

[30] Ram, P.C., Singh, A. and Takhar, H.S., Effects of Hall and ionslip currents on convective flow in a rotating fluid with a wall temperature oscillation, Magnetohydrodynamics and Plasma Research J., 5, 1-16 (1995).

[31] Takhar, H.S. , and Jha, B.K. Effects of Hall and ion-slip currents on MHD flow past an impulsively started plate in a rotating system, J. Magnetohydrodynamics and Plasma Research,8, 61-72 (1998).

[32] Kinyanjui, M., Chaturvedi, N. and Uppal, S.M., MHD Stokes problem for a vertical infinite plate in a dissipative rotating fluid with Hall current, Energy Conversion and Management, 39, 541-548 (1998).

[33] Takhar, H.S., Chamkha, A.J. and Nath, G.: MHD flow over a moving plate in a rotating fluid with magnetic field, Hall currents and free stream velocity, Int. J. Engineering Science 40, 1511-1527 (2002).

[34] Naroua, H., H.S. Takhar, P.C. Ram, T. A. Bég, O. Anwar Bég and R. Bhargava, Transient rotating hydro-magnetic partially-ionized heat-generating gas dynamic flow with Hall/Ionslip current effects: finite element analysis, Int. J. Fluid Mechanics Research, 34, 6, 493-505 (2007).

[35] Ghosh, S.K., Hall effect on unsteady hydro-magnetic flow in a rotating channel permeated by an inclined magnetic field in the presence of an oscillator, Czech. J. Physics, 49, 4, 465-472 (1999).

[36] Ghosh, S.K. and Pop, I., An analytical approach to MHD plasma behaviour of a rotating environment in the presence of an inclined magnetic field as compared to excitation frequency, Int. J. Applied Mechanics Engineering, 11, 4, 845-856 (2006).

[37] Bear, J., Dynamics of Fluids in Porous Media, Dover, New York (1988).

[38] H. S. Takhar, R. Bhargava, S. Rawat, T. A. Bég, O. Anwar Bég and T.K. Hung, Biomagnetic hydrodynamics in a 2-dimensional non-Darcian porous medium: finite element study, J. Theoretical and Applied Mechanics, 37, 2, 59-76 (2007).

[39] Takhar. H.S. and Ram P.C.: Effects of Hall currents on hydro-magnetic free convective flow through a porous medium, Astrophysics and Space Science J.. 192 45-51 (1992).

[40] Prasad, V.R, Takhar, H.S., Zueco, J., Ghosh, S.K. and Bég, O. Anwar, Numerical study of hydro-magnetic viscous plasma flow with Hall current effects in rotating porous media, Invited paper, 53^{rd} Congress ISTAM, University College of Engineering, Osmania University, Hyderabad, India, December, 147-157 (2008).

[41] Bég, O. Anwar, Zueco, J. and Takhar, H.S., Unsteady magnetohydrodynamic Hartmann-Couette flow and heat transfer in a Darcian channel with Hall current, ionslip, viscous and Joule heating effects: Network numerical solutions, Communications in Nonlinear Science Numerical Simulation, 14, 1082-1097 (2009).

[42] Bég, O. Anwar, Zueco, J. and Takhar, H.S., Laminar free convection from a continuously-moving vertical surface in thermally-stratified non-Darcian high porosity medium, Int. Communications Heat Mass Transfer, 35, 810-816 (2008).

[43] Bég, O. Anwar, Takhar, H.S., Zueco, J., Sajid, A. and Bhargava, R., Transient Couette flow in a rotating non-Darcian porous medium parallel plate configuration: network simulation method solutions, Acta Mechanica, 200, 129-144 (2008).

[44] Pspice 6.0. Irvine, California 92718. Microsim Corporation, 20 Fairbanks (1994).

[45] R. Bhargava, S. Rawat, H.S. Takhar and Bég, O. Anwar, Pulsatile magneto-biofluid flow and mass transfer in a non-Darcian porous medium channel, Mecannica 42, 247-262 (2007).

[46] Bég, O. Anwar, Takhar, H.S., Bhargava, R., Rawat, S. and Prasad, V.R., Numerical study of heat transfer of a third grade viscoelastic fluid in non-Darcy porous media with thermophysical effects, Physica Scripta, 77, 1-11 (2008).

[47] Bég, O. Anwar, Bhargava, R., Rawat, S., Halim, K. and Takhar, H.S., Computational modeling of biomagnetic micropolar blood flow and heat transfer in a two-dimensional non-Darcian porous medium, Meccanica, 43, 391-410 (2008).

[48] Bég, O. Anwar, Takhar, H.S. and Bég, Tasveer A., Bhargava, R. and Rawat, S., Nonlinear magneto-heat transfer in a fluid particle suspension flowing in a non-Darcian channel with heat source and buoyancy effects: Numerical study, J. King Abdul Aziz University: Engineering Sciences, 19, 1, 63-88 (2008).

[49] Bathe, K.J., Finite Element Procedures, Prentice-Hall, New Jersey (1996).

Submitted in July 2013.

Simulacija konačnim elementima i električnom mrežom obrtnog magnetofluidnog tečenja u nelinearnoj poroznoj sredini sa nagnutim magnetnim poljem i Hall-ovim tečenjem

Dat je matematički model za viskozno hidromagnetno tečenje kroz hibridnu ne-Darcy poroznu sredinu obrtnog generatora. Sistem je simuliran kao stacionarno nestišljivo tečenje nestišljivim nelinearnim poroznim režimom ubacenim medju paralelne ploče generatora u obrtnom sistemu referencije u prisustvu jakog nagnutog magnetskog polja. Gradijentni član je uključen koji je funkcija uzduže koordinate. Opšte jednačine obrtnog viskoznog magnetohidrodinamičkog tečenja su prikazane. Zanemarujući članove konvektivnog ubrzanja 2D jednačine su izvedene koje uključuju komponente gustine struje, efekte otpora porozne sredine, komponenata Lorentz-ove sile otpora i efekte Hall-ovog toka. Koristeci podesnu grupu bezdimenzionalnih promenljivih, jednačine količine kretanja za primarno i sekundarno tečenje su pruž. Pokazano je da su one kontrolisane sa šest fizičkih parametara– Hartmann-ovim brojem (HA), Hall-ovim tekućim parametrom (NH), Darcy-jevim brojem (Da), Forchheimer-ovim brojem (FS), Ekman-ovim brojem (Ek), i bezdimenzionim parametrom gradijenta pritiska (NP), sa dodatkom samo jednog geometrijskog parametra-orijentacijom primenjenog magnetskog polja (θ). Nekoliko posebnih slučajeva su izdvojeni iz opšteg modela, uključujući neporozni slučaj proučen ranije Ghosh-om i Pop-om (2006.). Numeričko rešenje je predstavljeno nelinearnim spregnutim obicnim diferencijalnimh jednačinama korišćenjem kako **Network Simulation Method** tako i **Metode konačnih elemenata**, postižući izvrsnu saglasnost. Uz to vrlo dobra saglasnost je dobijena sa ranijim analitičkim rešenjem Ghosh-a i Pop-a (2006.) za odabrane Ha, Ek i Nh vrednosti. Ispitujemo u detalje učinke magnetskog polja, obrtanja, Hall-ove struje, zapreminskim otporom porozne matrice, poroznom impedancom drugog reda, gradijenta pritiska a, takodje, i smičućim naponima na pločama. Vidi se da se osnovna brzina smanjuje sa povećanjem Hall-ovim tekućim parametrom (NH), dok je obrnuto primećeno za sekundarnu brzinu.

doi:10.2298/TAM1401001B Math. Subj. Class.: 65L60; 74L60; 74S05.